Mapping Delocalization of Impurity Bands across Archetypal Mott-Anderson Transition

M. Parzer,[1,*] F. Garmroudi,[2,†] A. Riss,[1] T. Mori,[3,4] A. Pustogow,[1] and E. Bauer[1]
[1]Institute of Solid State Physics, Technische Universität Wien, 1040 Vienna, Austria
[2]Materials Physics Applications - Quantum, Los Alamos National Laboratory, Los Alamos, New Mexico 87545, USA
[3]International Center for Materials Nanoarchitectonics (WPI-MANA), National Institute for Materials Science (NIMS), Tsukuba, Japan
[4]Graduate School of Pure and Applied Science, University of Tsukuba, Tsukuba, Japan

(Received 16 November 2024; accepted 9 July 2025; published 6 August 2025)

Tailoring charge transport in solids on demand is the overarching goal of condensed-matter research as it is crucial for electronic applications. Yet, often the proper tuning knob is missing and extrinsic factors such as impurities and disorder impede coherent conduction. Here, we control the very buildup of an electronic band from impurity states within the pseudogap of ternary $Fe_{2-x}V_{1+x}Al$ Heusler compounds via reducing the Fe content. Our density-functional theory calculations combined with specific heat and electrical resistivity experiments reveal that, initially, these states are Anderson-localized at low V concentrations $0 < x < 0.1$. As x increases, we monitor the formation of mobility edges upon the archetypal Mott-Anderson transition and map the increasing bandwidth of conducting states by thermoelectric measurements. Ultimately, delocalization of charge carriers in fully disordered V_3Al results in a resistivity exactly at the Mott-Ioffe-Regel limit that is perfectly temperature-independent up to 700 K—more constant than constantan.

DOI: 10.1103/fz9j-bj87

Introduction—The periodic arrangement of atoms in crystals forms energy bands, where electrons behave as extended Bloch waves. In single atoms, however, electrons occupy localized energy levels. It was Sir Nevill Mott who first approached the fundamental question in condensed-matter physics of band formation, transitioning from localized insulating states to delocalized metallic states. He argued that as two atoms move closer, at a certain point, a critical threshold is reached where the screening of ions by neighboring electrons becomes strong enough to delocalize them [1].

In doped semiconductors, a similar, but more realistic, transition occurs. At low doping levels, electrons remain trapped at impurity sites, but increasing dopant concentration leads to a critical concentration, x_c, where an insulator-metal phase transition occurs [1,2]. Additionally, correlations among the electrons can localize and split the narrow impurity bands (IBs) by an energy gap $\Delta = U - W$, with U being the Coulomb interaction and W the band width. In parallel to Mott's work, Anderson developed a theory of disorder-induced localization of electrons in matter due to their wavelike nature [3]. In its essence, Anderson localization describes the absence of diffusion of wavelike objects due to the multiple scattering events and quantum interference of self-intersecting scattering paths [4–8]. In low-doped semiconductors, both Mott and Anderson localization—the latter arising from the inherently random distribution of impurity atoms on the ordered crystal lattice—are believed to contribute to the insulating nature of the IB [1,9]. Figure 1 illustrates both these localization mechanisms and the way in which delocalization has been theoretically predicted to take place: at the critical concentration x_c, two mobility edges E_c emerge in the center of the IB. These critical energies separate localized states in the band tails from delocalized ones in the center [10].

The delocalization of IBs and their effect on electronic transport remain an important question, given the widespread use of dopant atoms with in-gap impurity states to control the physical properties of semiconductors in various electronic devices [11–14]. However, up until now, extensive investigation of the Mott-Anderson transition (MAT) in IBs has frequently been hindered by the low solubility of dopant atoms and the fact that the IBs usually hybridize with the bulk conduction bands. This has hindered the unambiguous analysis of the MAT in IBs, resulting, for instance, in the so-called exponent puzzle for the critical exponent describing the universality of the transition [15,16].

Here, we successfully map the delocalization of IBs in semiconducting $Fe_{2-x}V_{1+x}Al$ Heusler compounds, highlighting the impact of disorder on the broadening of the impurity band. This system offers exceptional tunability of the chemical composition ($-1 \leq x \leq 2$) within a similar

*Contact author: michael_parzer@yahoo.de
†Contact author: f.garmroudi@gmx.at

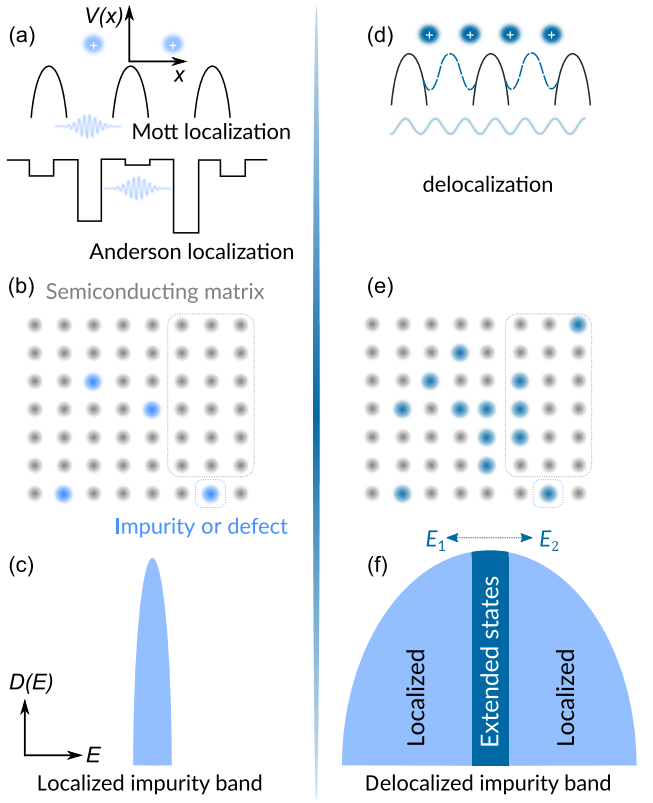

FIG. 1. Sketch of the Mott-Anderson transition. (a) Mott-type and Anderson-type charge localization mechanisms in solids. (b) Semiconducting matrix with isolated impurities and (c) a corresponding localized IB. (d) Atomic potentials, hosting extended Bloch states. (e) Semiconducting matrix with percolation of impurities, and (f) a partly delocalized IB.

cubic structure, ranging from Fe_3Al with the partially disordered $D0_3$ structure up to V_3Al with the fully disordered A2 structure [see Fig. 2(a)]. Crucially, the IB arises within the center of the gap and its bandwidth remains remarkably narrow up to large concentrations of x ($\approx$0.2 eV at $x = 0.074$). This confines the electronic transport at low temperatures to the IB states, allowing one to map the MAT from the fully insulating to the disordered and correlated metal regime. Recently, we studied electronic transport in stoichiometric Fe_2VAl, where a MAT arises from thermally quenched antisite disorder and boosts thermoelectric performance [13]. However, the concentration of defects, which can be induced via thermal quenching, is limited by rapid ordering during the quenching process and the frozen disordered structures comprise a combination of various different defects, promoting hybridization with the bulk bands and turning the system immediately metallic. Therefore, composition tuning in $Fe_{2-x}V_{1+x}Al$ across the whole range, $-1 \leq x \leq 2$, presents a much more controlled way of probing charge transport across the MAT.

The Heusler compound Fe_2VAl, crystallizing in the fully ordered $L2_1$ structure, has long been known as a promising thermoelectric material for near-ambient temperature applications [18–21], owing to its narrow pseudogap in the electronic structure. Over the recent years, various substitution studies have been performed to optimize the position of the Fermi energy and to tailor the band structure itself, resulting in outstanding thermoelectric power factors that rival or exceed those of state-of-the-art Bi_2Te_3 thermoelectrics [22–25].

A highly unconventional doping dependence of the thermoelectric properties has been reported for off-stoichiometric, self-substituted $Fe_{2-x}V_{1+x}Al$ [26,27]. Figure S1 in Supplemental Material (SM) [28] compares the Seebeck coefficient S as a function of the valence electron concentration per atom (VEC) for $Fe_{2-x}V_{1+x}Al$ and various substituted Fe_2VAl-based compounds with different substitution elements. Typically, for VEC < 6 (corresponding to p-type doping) S is expected to be positive, and for VEC > 6 (n-type doping) $S < 0$ is expected. This trend is indeed observed in all known substituted compounds except for $Fe_{2-x}V_{1+x}Al$, where an entirely opposite behavior emerges. Moreover, Naka *et al.* reported a composition-induced metal-insulator quantum phase transition in V-rich $Fe_{2-x}V_{1+x}Al$ and a ferromagnetic quantum critical point in Fe-rich $Fe_{2-x}V_{1+x}Al$ [17,54], yet the exact mechanisms behind these transitions remain unclear. Here, we demonstrate that the origin of these quantum phase transitions and the highly unconventional doping behavior can be traced back to the delocalization of narrow IBs right next to E_F. Crucially, using temperature-dependent thermoelectric transport measurements we quantitatively map the width of the delocalized IB as a function of the impurity concentration.

To obtain insight into the states around E_F relevant for charge transport, we performed density-functional theory (DFT) calculations on supercells of substituted $Fe_{2-x}V_{1+x}Al$ with varying concentration of defects. Figure 2(b) displays the density of states (DOS) around E_F for $x = 0$, 0.037, 0.074. It is evident that for $x = 0 \rightarrow 0.037$, narrow and highly localized impurity states emerge within the pseudogap at the lower edge of the dispersive conduction band (CB). As the concentration of V antisites on the two Fe sublattices continues to increase, these states gradually broaden, eventually filling the entire pseudogap and transforming the system into a metal. However, the periodic boundary conditions (Bloch's theorem) imposed by the supercell approach and the lack of accounting for the decoherence of the wave functions prevent an accurate description of the Anderson-localized nature of these states. Thus, simple DFT calculations can only predict that there exist impurity states but not whether and to which extent they are localized.

On the other hand, examining composition- and temperature-dependent electronic transport of $Fe_{2-x}V_{1+x}Al$, displayed in Figs. 2(c)–2(e), reveals clear evidence for the Anderson-localized nature of these IBs as the low-temperature conductivity drops by several orders of

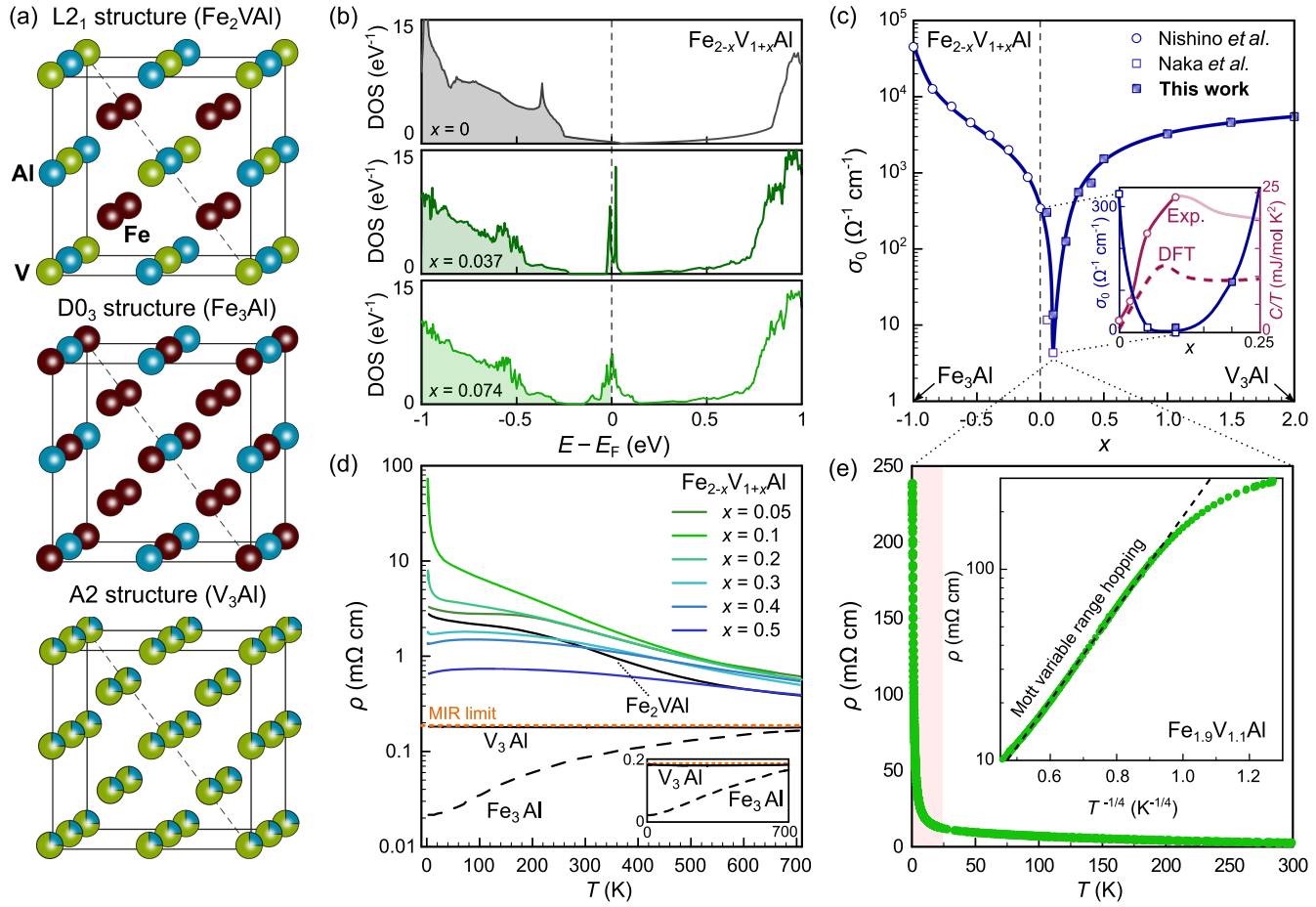

FIG. 2. Structure and electronic transport of $Fe_{2-x}V_{1+x}Al$ system. (a) Crystal structures of ternary Heusler compound Fe_2VAI crystallizing in the fully ordered $L2_1$ structure, binary Fe_3Al in the partly disordered $D0_3$ structures, and V_3Al in the fully disordered A2 structure. (b) Densities of states of $Fe_{2-x}V_{1+x}Al$ from DFT supercell calculations with $x = 0$, 0.037, 0.074. (c) Composition-dependent electrical conductivity at $T = 2$ K of $Fe_{2-x}V_{1+x}Al$ over the whole compositional phase space, from $-1 \leq x \leq 2$. A distinct minimum is observed at $x = 0.1$. Inset shows a magnified view of the conductivity minimum alongside the density of states at the Fermi level derived from specific heat data [17] and our DFT calculations, both showing a maximum instead. (d) Temperature-dependent resistivity $\rho(T)$ of $Fe_{2-x}V_{1+x}Al$ close to the significant minimum ($x = 0.1$–0.5), together with the two end points of the composition transition. Notably, Fe_3Al shows metallic behavior, while the resistivity of V_3AI is completely flat, with a residual resistivity ratio of ≈0.98, which is right at the Mott-Ioffe-Regel (MIR) limit (dotted red line), to which Fe_3Al converges at high temperatures. The inset shows $\rho(T)$ of the binary compounds on linear scale. (e) Signatures of Mott-Anderson charge localization in $\rho(T)$ of $Fe_{1.9}V_{1.1}Al$, measured down to 0.39 K. An extremely sharp upturn of $\rho(T)$ takes place below $T \approx 20$ K, consistent in with Mott variable range hopping (inset) in a broad range of temperatures.

magnitude and exhibits a sharp minimum at $x \approx 0.1$ [see Fig. 2(c)]. The inset in Fig. 2(c) compares the composition-dependent DOS at the Fermi level $D(E_F)$ obtained from DFT and specific heat data (C/T) [17] with the conductivity at $T = 2$ K. While, both DFT calculations and C/T data reveal a peak at $x = 0.1$ associated with the IBs, $\sigma_{2\,K}$ vanishes and only starts to increase at $x > 0.1$ when the impurities start to form a "real," delocalized band.

Temperature-dependent resistivity curves for several different compositions across a wide range of temperatures and compositional phase space are presented in Fig. 2(d). Focusing first on the end compounds, the magnetic metal Fe_3Al exhibits a metallicklike resistivity, $d\rho/dT > 0$, well described by the Bloch-Wilson law for $T < T_C$ (see SM [28]), with $T_C \approx 740$ K. On the other hand, V_3Al with the fully disordered A2 structure (see Ref. [55]) shows a negligible, negative temperature dependence of $\rho(T)$ with a residual resistivity ratio of ≈0.98, aligning with the phenomenological Mooij criterion [29–31] (see also Fig. S2 in SM [28]). Note that $\rho(T)$ of Fe_3Al saturates toward the value of V_3AI, which lies almost exactly at the Mott-Ioffe-Regel (MIR) limit (red dotted line), even in a nonlogarithmic plot [inset Fig. 2(d)]. The MIR limit states that the charge carrier mean free path is limited by the interatomic distance $k_F l_{min} \sim 2\pi$, where k_F is the Fermi wave vector and l_{min} the minimal mean free path. For spherical Fermi surfaces, Calandra and Gunnarsson

derived an expression [56,57],

$$\rho_{\mathrm{MIR}} = \frac{3\pi^2\hbar}{e^2 k_{\mathrm{F}}^2 l_{\mathrm{min}}}. \quad (1)$$

Assuming $k_{\mathrm{F}} \approx \pi/a$ and using the experimental lattice parameter of V_3Al, this yields $\rho_{\mathrm{MIR}} \approx 187\ \mu\Omega\,\mathrm{cm}$ [red dotted line in Fig. 2(d)], which almost perfectly coincides with the temperature-independent resistivity value of V_3Al $\rho(T) \approx \mathrm{const} \approx 180\ \mu\Omega\,\mathrm{cm}$ up to 700 K. Notably, $\rho(T)$ of this fully disordered metal is more constant than in constantan, with $\rho_{300\ \mathrm{K}}/\rho_{4\ \mathrm{K}} \approx 0.98$ and even approaching its low-temperature resistivity above room temperature, $\rho_{700\ \mathrm{K}}/\rho_{4\ \mathrm{K}} \approx 0.997$.

In the ternary system Fe_2VAl, a deep pseudogap develops around the Fermi energy, which leads to a semiconductor-like resistivity, $d\rho(T)/dT$, that can be mainly attributed to the thermal activation of charge carriers across the narrow pseudogap [58,59], although recently it has been shown that charge carrier scattering may also play an important role owing to residual intrinsic antisite exchange defects [60]. Notably, $\rho(T)$ increases further by more than an order of magnitude when additional V atoms are substituted on the Fe sites in $Fe_{1.9}V_{1.1}Al$, with a pronounced upturn at the lowest temperatures. Figure 2(e) shows a linear plot of $\rho(T)$ of $Fe_{1.9}V_{1.1}Al$ with measurements down to $T = 0.39$ K. The extremely sharp increase of $\rho(T)$ below ≈20 K is consistent with the presence of Anderson-localized states around E_{F} [see inset, Fig. 2(e)], although at the lowest temperatures, $T \lesssim 1.2$ K, $\rho(T)$ deviates significantly from variable range hopping behavior and can instead be described phenomenologically by a simple power law $\rho(T) \propto T^{-\alpha}$, with $\alpha = 1.3$–1.4, consistent with what has been reported by Naka *et al.* [17] and also, e.g., in doped silicon near the MAT [61–63].

At low temperatures, when thermally activated hopping of electrons from one localized impurity to the next, which are far apart in real space but close in energy, dominates, a temperature dependence $\rho(T) \propto \exp[(T_0/T)^{1/4}]$ is expected in three dimensions—commonly known as "Mott variable range hopping." Here, T_0 is the characteristic temperature, which depends inversely on the localization length

$$\xi_{\mathrm{L}} = \left(\frac{1}{18} D(E_{\mathrm{F}}) k_{\mathrm{B}} T_0\right)^{-1/3}. \quad (2)$$

The localization length indicates the exponential decay of the wave function $|\Psi(r)|^2 \sim \exp(-|r - r_0|/\xi_{\mathrm{L}})$ at an impurity site r_0. By fitting the slope of $\ln\rho$ versus $T^{-1/4}$ of $Fe_{1.9}V_{1.1}Al$ at low temperatures, T_0 is obtained as ≈490 K. Furthermore, using $D(E_{\mathrm{F}})$, derived from C/T data from Ref. [17], leads to a localization length $\xi_{\mathrm{L}} \approx 12$ nm, equaling about 21 unit cells. If one considers that for $Fe_{1.9}V_{1.1}Al$ about one impurity is present in every three unit cells, this suggests that already a significant overlap of the Anderson-localized wave functions exists. As will be demonstrated below, using temperature-dependent thermoelectric measurements, we confirm the existence of a delocalized regime of the IB and quantitatively assess its bandwidth W, which is not possible by merely investigating $\rho(T)$. We also performed measurements of the Hall mobility, which are presented in SM [28] and which qualitatively agree with both the conclusions drawn from the analysis of $\rho(T)$ above and $S(T)$ below.

Figure 3 shows $S(T)$ of $Fe_{2-x}V_{1+x}Al$ with $0.05 \le x \le 0.5$. For $x = 0.05$, the impurity states remain fully localized and do not actively contribute themselves to the transport properties. Instead, $S(T)$ is governed by the dispersive CB states up to 230 K, where holes from the dispersive valence band (VB) states are thermally activated and bipolar conduction takes over (see also SM [28]). As $x \ge 0.1$, a pronounced positive peak of $S(T)$ develops at low temperatures, which we assign to delocalization of the IB. To model the contribution of a (partly) delocalized IB to the Seebeck coefficient, a band with a finite width W was integrated into the two-parabolic band modeling framework commonly employed to understand charge transport in pristine Fe_2VAl and conventional doping scenarios [23,32,64]. For parabolic bands, the energy-dependent transport function $\Sigma(E) = D(E)v(E)^2\tau(E)$ increases linearly at the band edge $\Sigma(E) \propto E$ [65].

For the delocalized IB with finite width W, we developed a model in which $\Sigma(E)$ increases at either side of the mobility edge with

$$\Sigma(E,T) = \Sigma_0(T)\left(\frac{E - E_c}{k_{\mathrm{B}}T}\right)^{\nu}. \quad (3)$$

Here, ν is the critical exponent of the Anderson transition that can vary between 0.5 and 2, depending on compensation and band hybridization [16]. In our model, the entirety of the IB can be engineered using expressions following Eq. (3) to yield a single continuously differentiable function (for details, see SM [28]). Finally, the contribution of the entire IB to the transport properties can be evaluated from three independent parameters: (i) its bandwidth W, its maximum Σ_0, and (iii) the position of E_{F}.

$\Sigma(E)$ of the parabolic bands and the delocalized IB are then used to numerically solve the transport integrals and calculate the Seebeck coefficient,

$$S(T) = \frac{k_{\mathrm{B}}}{eT}\frac{\int_{-\infty}^{\infty}\Sigma(E)(E-\mu)(-\partial f/\partial E)dE}{\int_{-\infty}^{\infty}\Sigma(E)(-\partial f/\partial E)dE}, \quad (4)$$

with $f(E,\mu,T)$ and $\mu(T)$ being the Fermi-Dirac distribution and the chemical potential, respectively; the numerator in Eq. (4) represents the electrical conductivity. Since multiple bands contribute to the transport properties, the single-band contributions S_i have to be weighted with their respective conductivities σ_i,

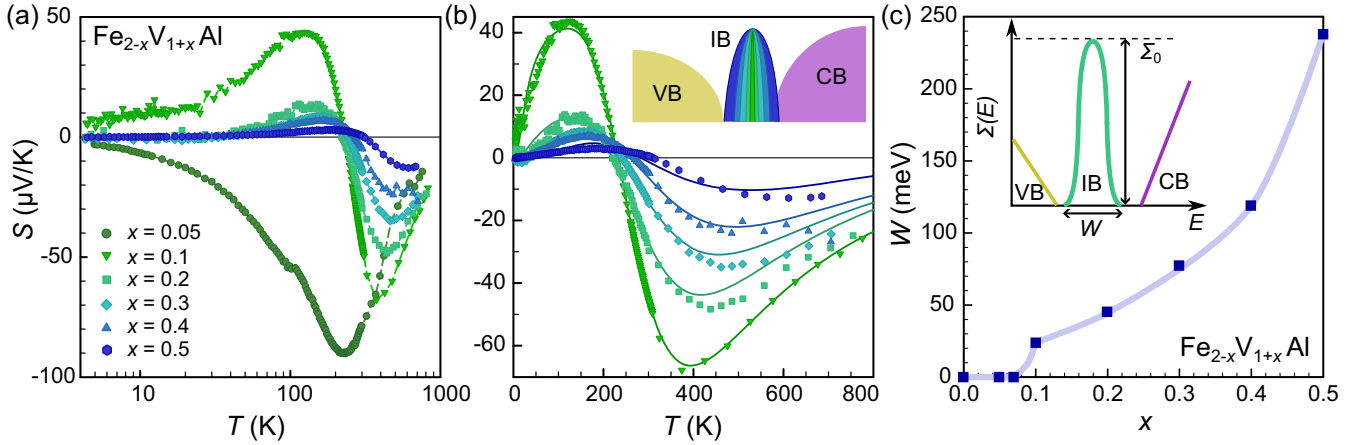

FIG. 3. Mapping delocalization of impurity bands via thermoelectric transport. (a) Temperature-dependent Seebeck coefficient $S(T)$ of $Fe_{2-x}V_{1+x}Al$ with $x = 0.05$–0.5. For $x = 0.05$, the impurities merely act as fully localized donor states, placing E_F right below the dispersive conduction band [see Fig. 2(b)] and leading to a negative $S(T)$ over the entire temperature range. As x increases up to 0.1, a distinct positive maximum develops around 120 K, which gets progressively smeared out and shifted toward higher temperatures with increasing x. (b) Experimental $S(T)$ and least-square fits (solid lines) employing a three-band model with parabolic valence and conduction bands and a delocalized impurity band confined to a width W. (c) Quantitative mapping of the composition dependence of W with a progressive broadening at $x > 0.1$. Inset shows a sketch of the energy-dependent transport distribution function $\Sigma(E)$ of our model.

$$S_{\mathrm{tot}} = \frac{\sum_i S_i \sigma_i}{\sum_i \sigma_i}, \tag{5}$$

where $i = \{\mathrm{VB}, \mathrm{CB}, \mathrm{IB}\}$. Equation (5) was fitted to the experimental $S(T)$ in the following way. First, $Fe_{1.9}V_{1.1}Al$, with the most pronounced second peak in $S(T)$, was fitted [Fig. 3(b)]. Here, the fit parameters are the two energy gaps between the IB center and the VB and CB, Δ_{VB} and Δ_{CB}, the effective mass ratio between the CB and VB, $m_{\mathrm{CB}}/m_{\mathrm{VB}}$, as well as W, Σ_0, and the position of E_F with respect to the IB center. In a second step, all these parameters, except for the bandwidth W, were fixed. Then, all the measured curves for the remaining samples were modeled and perfectly reproduced in a single-parameter fit, highlighting the robustness of our modeling approach and the obtained parameter values. Further details regarding the fitting procedure and the underlying charge transport model are presented in SM [28].

With respect to the IB center, the energy gaps were determined as 120 meV toward the valence band and 100 meV toward the conduction band edge, highlighting that the impurity band forms in the middle of the gap, in agreement with our DFT results. The effective mass ratio of the two bands $m_{\mathrm{CB}}/m_{\mathrm{VB}}$ is obtained as ≈ 2, in good agreement with previous parabolic band modeling analyses of Fe_2VAl-based thermoelectrics [64]. Most importantly, for $Fe_{1.9}V_{1.1}Al$, our analysis reveals an extremely narrow region ($W \approx 24$ meV) of the IB and E_F positioned right next to the center of the IB, in striking agreement with the DFT-derived DOS. As x increases, our modeling scheme accurately predicts the delocalization of the IB as W progressively increases up to 240 meV in $Fe_{1.5}V_{1.5}Al$, as shown in Fig. 3(c).

In conclusion, our study provides a thorough investigation of the $Fe_{2-x}V_{1+x}Al$ Heusler system, focusing on the composition-induced Mott-Anderson transition. By examining a wide range of compositions from Fe_3Al to V_3Al, we identified a profound conductivity minimum in the V self-substituted Heusler compound $Fe_{1.9}V_{1.1}Al$. Temperature-dependent resistivity measurements near this stoichiometry reveal Mott variable range hopping behavior with a localization length $\xi_L \approx 12$ nm. The temperature-dependent Seebeck coefficient was measured over a wide range of temperatures and compositions and a charge transport model was developed to accurately describe thermoelectric transport in delocalized impurity bands. Analyzing various $S(T)$ datasets within this modeling framework, we successfully capture and quantitatively map the delocalization of IBs in $Fe_{2-x}V_{1+x}Al$. Our findings emphasize the value of thermoelectric transport measurements in probing the electronic structure and transport mechanisms in complex materials, especially when paired with appropriate multiband fitting models. This work not only advances the understanding of Fe_2VAl-based thermoelectrics and solves the issue of the unconventional doping behavior in $Fe_{2-x}V_{1+x}Al$, but also provides a robust framework for studying similar transitions in other materials.

Acknowledgments—The authors thank V. Dobrosavljevic and S. Fratini for fruitful discussions. Financial support for M. P., F. G., A. R., T. M., and E. B. came from the Japan Science and Technology Agency (JST), program MIRAI, JPMJMI19A1. The computational

results presented have been achieved using the Vienna Scientific Cluster (VSC). The authors acknowledge TU Wien Bibliothek for financial support through its Open Access Funding Programme. F. G. acknowledges a Director's Postdoctoral Fellowship through the Laboratory and Directed Research & Development (LDRD) program.

[1] N. Mott, On the transition to metallic conduction in semiconductors, Can. J. Phys. **34**, 1356 (1956).
[2] N. F. Mott and W. Twose, The theory of impurity conduction, Adv. Phys. **10**, 107 (1961).
[3] P. W. Anderson, Absence of diffusion in certain random lattices, Phys. Rev. **109**, 1492 (1958).
[4] M. Cutler and N. F. Mott, Observation of Anderson localization in an electron gas, Phys. Rev. **181**, 1336 (1969).
[5] T. Schwartz, G. Bartal, S. Fishman, and M. Segev, Transport and Anderson localization in disordered two-dimensional photonic lattices, Nature (London) **446**, 52 (2007).
[6] G. Roati, C. D'Errico, L. Fallani, M. Fattori, C. Fort, M. Zaccanti, G. Modugno, M. Modugno, and M. Inguscio, Anderson localization of a non-interacting Bose–Einstein condensate, Nature (London) **453**, 895 (2008).
[7] V. Dobrosavljevic, N. Trivedi, and J. M. Valles Jr, *Conductor Insulator Quantum Phase Transitions* (Oxford University Press, USA, 2012), Chap. 1.
[8] M. Segev, Y. Silberberg, and D. N. Christodoulides, Anderson localization of light, Nat. Photonics **7**, 197 (2013).
[9] D. Belitz and T. Kirkpatrick, The Anderson-Mott transition, Rev. Mod. Phys. **66**, 261 (1994).
[10] N. Mott, Electrons in disordered structures, Adv. Phys. **16**, 49 (1967).
[11] E. Prati, M. Hori, F. Guagliardo, G. Ferrari, and T. Shinada, Anderson–Mott transition in arrays of a few dopant atoms in a silicon transistor, Nat. Nanotechnol. **7**, 443 (2012).
[12] Z. Yu, Impurity-band transport in organic spin valves, Nat. Commun. **5**, 4842 (2014).
[13] Anderson transition in stoichiometric Fe_2VAl: high thermoelectric performance from impurity bands.
[14] W.-G. D. Ho, P. Zhang, K. Haule, J. M. Jackson, V. Dobrosavljević, and V. V. Dobrosavljevic, Quantum critical phase of FeO spans conditions of Earth's lower mantle, Nat. Commun. **15**, 3461 (2024).
[15] H. Stupp, M. Hornung, M. Lakner, O. Madel, and H. v. Löhneysen, Possible solution of the conductivity exponent puzzle for the metal-insulator transition in heavily doped uncompensated semiconductors, Phys. Rev. Lett. **71**, 2634 (1993).
[16] E. G. Carnio, N. D. Hine, and R. A. Römer, Resolution of the exponent puzzle for the Anderson transition in doped semiconductors, Phys. Rev. B **99**, 081201(R) (2019).
[17] T. Naka, A. M. Nikitin, Y. Pan, A. de Visser, T. Nakane, F. Ishikawa, Y. Yamada, M. Imai, and A. Matsushita, Composition induced metal–insulator quantum phase transition in the Heusler type Fe_2VAI, J. Phys. Condens. Matter **28**, 285601 (2016).
[18] V. Pecunia, S. R. P. Silva, J. D. Phillips, E. Artegiani, A. Romeo, H. Shim, J. Park, J. H. Kim, J. S. Yun, G. C. Welch *et al.*, Roadmap on energy harvesting materials, J. Nonlinear Opt. Phys. Mater. **6**, 042501 (2023).
[19] Y. Nishino, S. Deguchi, and U. Mizutani, Thermal and transport properties of the Heusler-type $Fe_2VAl_{1-x}Ge_x$ ($0 \leq x \leq 0.20$) alloys: Effect of doping on lattice thermal conductivity, electrical resistivity, and seebeck coefficient, Phys. Rev. B **74**, 115115 (2006).
[20] M. Mikami, K. Kobayashi, T. Kawada, K. Kubo, and N. Uchiyama, Development and evaluation of high-strength Fe_2VAl thermoelectric module, Jpn. J. Appl. Phys. **47**, 1512 (2008).
[21] M. Mikami, Y. Kinemuchi, K. Ozaki, Y. Terazawa, and T. Takeuchi, Thermoelectric properties of tungsten-substituted Heusler Fe_2VAl alloy, J. Appl. Phys. **111**, 093710 (2012).
[22] H. Miyazaki, S. Tanaka, N. Ide, K. Soda, and Y. Nishino, Thermoelectric properties of Heusler-type off-stoichiometric $Fe_2V_{1+x}Al_{1-x}$ alloys, Mater. Res. Express **1**, 015901 (2013).
[23] F. Garmroudi, A. Riss, M. Parzer, N. Reumann, H. Müller, E. Bauer, S. Khmelevskyi, R. Podloucky, T. Mori, K. Tobita *et al.*, Boosting the thermoelectric performance of Fe_2VAI-type Heusler compounds by band engineering, Phys. Rev. B **103**, 085202 (2021).
[24] F. Garmroudi, M. Parzer, A. Riss, S. Beyer, S. Khmelevskyi, T. Mori, M. Reticcioli, and E. Bauer, Large thermoelectric power factors by opening the band gap in semimetallic Heusler alloys, Mater. Today Phys. **27**, 100742 (2022).
[25] E. Alleno, A. Diack-Rasselio, M. Talla Noutack, and P. Jund, Optimization of the thermoelectric properties in self-substituted Fe_2VAI, Phys. Rev. Mater. **7**, 075403 (2023).
[26] Y. Hanada, R. O. Suzuki, and K. Ono, Seebeck coefficient of $(Fe, V)_3Al$ alloys, J. Alloys Compounds **329**, 63 (2001).
[27] Y. Nishino and Y. Tamada, Doping effects on thermoelectric properties of the off-stoichiometric Heusler compounds $Fe_{2-x}V_{1+x}Al$, J. Appl. Phys. **115**, 123707 (2014).
[28] See Supplemental Material at http://link.aps.org/supplemental/10.1103/fz9j-bj87 for additional details on material characterization, supplemental (magneto-)transport measurements, and a comprehensive description of the fitting procedure, which includes Refs. [16,17,26,29–53].
[29] J. Mooij, Electrical conduction in concentrated disordered transition metal alloys, Phys. Status Solidi (a) **17**, 521 (1973).
[30] D. Di Sante, S. Fratini, V. Dobrosavljević, and S. Ciuchi, Disorder-driven metal-insulator transitions in deformable lattices, Phys. Rev. Lett. **118**, 036602 (2017).
[31] S. Ciuchi, D. Di Sante, V. Dobrosavljević, and S. Fratini, The origin of Mooij correlations in disordered metals, npj Quantum Mater. **3**, 44 (2018).
[32] B. Hinterleitner, F. Garmroudi, N. Reumann, T. Mori, E. Bauer, and R. Podloucky, The electronic pseudo band gap states and electronic transport of the full-Heusler compound Fe_2VAI, J. Mater. Chem. C **9**, 2073 (2021).
[33] R. Resel, E. Gratz, A. Burkov, T. Nakama, M. Higa, and K. Yagasaki, Thermopower measurements in magnetic fields up to 17 tesla using the toggled heating method, Rev. Sci. Instrum. **67**, 1970 (1996).
[34] B. Hinterleitner, P. Fuchs, J. Rehak, F. Garmroudi, M. Parzer, M. Waas, R. Svagera, S. Steiner, M. Kishimoto, R. Moser *et al.*, Stoichiometric and off-stoichiometric full Heusler $Fe_2V_{1-x}W_xAl$ thermoelectric systems, Phys. Rev. B **102**, 075117 (2020).

[35] F. Garmroudi, M. Parzer, A. Riss, N. Reumann, B. Hinterleitner, K. Tobita, Y. Katsura, K. Kimura, T. Mori, and E. Bauer, Solubility limit and annealing effects on the microstructure & thermoelectric properties of $Fe_2V_{1-x}Ta_xAl_{1-y}Si_y$ Heusler compounds, Acta Mater. **212**, 116867 (2021).

[36] P. Hohenberg and W. Kohn, Inhomogeneous electron gas, Phys. Rev. **136**, B864 (1964).

[37] W. Kohn and L. J. Sham, Self-consistent equations including exchange and correlation effects, Phys. Rev. **140**, A1133 (1965).

[38] G. Kresse and J. Hafner, *Ab initio* molecular dynamics for liquid metals, Phys. Rev. B **47**, 558 (1993).

[39] G. Kresse and J. Furthmüller, Efficiency of ab-initio total energy calculations for metals and semiconductors using a plane-wave basis set, Comput. Mater. Sci. **6**, 15 (1996).

[40] G. Kresse and J. Furthmüller, Efficient iterative schemes for *ab initio* total-energy calculations using a plane-wave basis set, Phys. Rev. B **54**, 11169 (1996).

[41] G. Kresse and D. Joubert, From ultrasoft pseudopotentials to the projector augmented-wave method, Phys. Rev. B **59**, 1758 (1999).

[42] J. P. Perdew, K. Burke, and M. Ernzerhof, Generalized gradient approximation made simple, Phys. Rev. Lett. **77**, 3865 (1996).

[43] M. Parzer, F. Garmroudi, A. Riss, S. Khmelevskyi, T. Mori, and E. Bauer, High solubility of Al and enhanced thermoelectric performance due to resonant states in Fe_2VAl_x, Appl. Phys. Lett. **120** (2022).

[44] T. Nakama, Y. Takaesu, K. Yagasaki, T. Naka, A. Matsushita, K. Fukuda, and Y. Yamada, Transport properties of Heusler compounds $Fe_{3-x}V_xAl$, J. Phys. Soc. Jpn. **74**, 1378 (2005).

[45] S. L. Dudarev, G. A. Botton, S. Y. Savrasov, C. Humphreys, and A. P. Sutton, Electron-energy-loss spectra and the structural stability of nickel oxide: An LSDA + U study, Phys. Rev. B **57**, 1505 (1998).

[46] B. L. Al'tshuler, A. G. Aronov, and D. E. Khmel'nitskiĭ, Negative magnetoresistance in semiconductors in the hopping conduction region, JETP Lett. **36**, 195 (1982), http://jetpletters.ru/ps/1333/article_20140.pdf.

[47] Y. Nishino, M. Kato, S. Asano, K. Soda, M. Hayasaki, and U. Mizutani, Semiconductorlike behavior of electrical resistivity in Heusler-type Fe_2VAl compound, Phys. Rev. Lett. **79**, 1909 (1997).

[48] M. E. Jamer, B. A. Assaf, G. E. Sterbinsky, D. Arena, L. H. Lewis, A. A. Saúl, G. Radtke, and D. Heiman, Antiferromagnetic phase of the gapless semiconductor V_3Al, Phys. Rev. B **91**, 094409 (2015).

[49] I. Zvyagin, On the theory of hopping transport in disordered semiconductors, Phys. Status Solidi (b) **58**, 443 (1973).

[50] D. Cvijović, The Bloch-Gruneisen function of arbitrary order and its series representations, Theor. Math. Phys. **166**, 37 (2011).

[51] M. Kato, Y. Nishino, U. Mizutani, and S. Asano, Electronic, magnetic and transport properties of $(Fe_{1-x}V_x)_3Al$ alloys, J. Phys. Condens. Matter **12**, 1769 (2000).

[52] M. Parzer, A. Riss, F. Garmroudi, J. de Boor, T. Mori, and E. Bauer, Seeband: A highly efficient, interactive tool for analyzing electronic transport data, arXiv:2409.06261.

[53] S. D. Kang and G. J. Snyder, Charge-transport model for conducting polymers, Nat. Mater. **16**, 252 (2017).

[54] T. Naka, K. Sato, M. Taguchi, T. Nakane, F. Ishikawa, Y. Yamada, Y. Takaesu, T. Nakama, and A. Matsushita, Ferromagnetic quantum singularities and small pseudogap formation in Heusler type $Fe_{2+x}V_{1-x}Al$, Phys. Rev. B **85**, 085130 (2012).

[55] R. Zhang, Z. Gercsi, M. Venkatesan, K. Rode, and J. M. D. Coey, Pauli paramagnetism of cubic V_3Al, CrVTiAl, and related 18-electron Heusler compounds with a group-13 element, Phys. Rev. B **103**, 174407 (2021).

[56] M. Calandra and O. Gunnarsson, Electrical resistivity at large temperatures: Saturation and lack thereof, Phys. Rev. B **66**, 205105 (2002).

[57] O. Gunnarsson, M. Calandra, and J. Han, Colloquium: Saturation of electrical resistivity, Rev. Mod. Phys. **75**, 1085 (2003).

[58] H. Okamura, J. Kawahara, T. Nanba, S. Kimura, K. Soda, U. Mizutani, Y. Nishino, M. Kato, I. Shimoyama, H. Miura *et al.*, Pseudogap formation in the intermetallic compounds $(Fe_{1-x}V_x)_3Al$, Phys. Rev. Lett. **84**, 3674 (2000).

[59] Y. Nishino, Electronic structure and transport properties of pseudogap system Fe_2VAI, Mater. Trans., JIM **42**, 902 (2001).

[60] F. Garmroudi, M. Parzer, A. Riss, A. Pustogow, T. Mori, and E. Bauer, Pivotal role of carrier scattering for semiconductorlike transport in Fe_2VAI, Phys. Rev. B **107**, L081108 (2023).

[61] N. Mott and M. Kaveh, Metal—insulator transition in doped silicon, Philos. Mag. B **47**, 577 (1983).

[62] A. Long and M. Pepper, The magnetic field induced metal-insulator transition in indium phosphide and silicon, Solid-State Electron. **28**, 61 (1985).

[63] W. N. Shafarman, D. W. Koon, and T. G. Castner, dc conductivity of arsenic-doped silicon near the metal-insulator transition, Phys. Rev. B **40**, 1216 (1989).

[64] S. Anand, R. Gurunathan, T. Soldi, L. Borgsmiller, R. Orenstein, and G. J. Snyder, Thermoelectric transport of semiconductor full-Heusler VFe_2AI, J. Mater. Chem. C **8**, 10174 (2020).

[65] A. Zevalkink, D. M. Smiadak, J. L. Blackburn, A. J. Ferguson, M. L. Chabinyc, O. Delaire, J. Wang, K. Kovnir, J. Martin, L. T. Schelhas *et al.*, A practical field guide to thermoelectrics: Fundamentals, synthesis, and characterization, Appl. Phys. Rev. **5** (2018).